Biosensors and Bioelectronics 142 (2019) 111555

Contents lists available at ScienceDirect

Biosensors and Bioelectronics

journal homepage: www.elsevier.com/locate/bios

Reepithelialization in focus: Non-invasive monitoring of epidermal wound healing *in vitro*

Lisa Kiesewetter[a,b,*], Laura Littau[a], Heike Walles[a,c], Aldo R. Boccaccini[d], Florian Groeber-Becker[a]

[a] Translational Center for Regenerative Therapies TLZ-RT, Fraunhofer-Institute for Silicate Research ISC, Neunerplatz 2, 97082, Würzburg, Germany
[b] Department Tissue Engineering & Regenerative Medicine (TERM), University Hospital Würzburg, 97070, Würzburg, Germany
[c] Core Facility Tissue Engineering, Otto-von-Guericke-University, Building 28, Pfälzerstr. 2, 39106, Magdeburg, Germany
[d] Institute of Biomaterials, Department of Materials Science and Engineering, University of Erlangen-Nürnberg, Cauerstr. 6, 91058, Erlangen, Germany

ARTICLE INFO

Keywords:
Impedance spectroscopy
Reconstructed human epidermis
Epidermal wound healing
Reepithelialization
Transepithelial electrical resistance

ABSTRACT

Up to today, *in vivo* studies are the gold standard for testing of new therapeutics for cutaneous wound healing. Alternative *in vitro* studies are mostly limited to two-dimensional cell cultures and thus only poorly reflect the complex physiological wound situation. Here we present a new three-dimensional wound model based on a reconstructed human epidermis (RHE). We introduce impedance spectroscopy as a time-resolved test method to determine the efficacy of wound healing non-destructively by focusing on the barrier function of the RHE as a main feature of intact skin. We assessed the skin barrier quantitatively and qualitatively by calculating the transepithelial electrical resistance (*TEER*), by fitting an equivalent circuit and by analyzing the single characteristic frequency. Upon wounding using a 2 mm biopsy punch, the impedance dropped significantly to 3.5% of the initial value. Impedance spectroscopy thereby proved to be a sensitive tool to distinguish between wounds of different sizes. The glucose and lactate concentration in the medium revealed an acute stress reaction of the wounded RHE (wRHE) in the first days after wounding. During monitoring of reepithelialization over fourteen days, the barrier fully recovered. Microscopy and histology images correlate well with these findings, revealing an active wound closure mostly completed by day seven after wounding. These wounded epidermal models can now be applied in therapeutic screenings and with the help of rapid screening by impedance spectroscopy, expensive and time-consuming imaging and histological methods as well as the use of animal models can be reduced.

1. Introduction

The reepithelialization step is crucial for wound recovery and for the human skin to regain functionality (Martin, 1997; Safferling et al., 2013), but might be impaired or even completely absent such as in the case of diseases or chronic wounds. Reepithelialization thus remains a point of focus in clinical research. However, most research in the field of wound healing is still performed using animal models or conventional 2D cell cultures employing cell lines or primary skin cells. Typically, reepithelialization is studied in 2D scratch assays, where a cell free area is generated in a confluent monolayer of keratinocytes, either by scratching using a pipette tip (Chen et al., 2014; Chmielowiec et al., 2007; Liang et al., 2007; Liu et al., 2009; Menger et al., 2011), removal by biopsy punch (Gonzalez-Andrades et al., 2016) or by taking a cylinder-shaped place holder during cell seeding, which is removed later after a confluent cell layer is reached (Liu et al., 2009). Most wound healing assays focus on the cellular migration as the limiting process and the closure of the scratch wound is monitored microscopically during further culture (Stamm et al., 2016). Compared to the situation *in vivo*, 2D cell cultures lack functionality such as the distinct high barrier present *in vivo* and biological appearance of the human skin, given by the stratification of the keratinocytes and the formation of a multilayered model including the strata basale, spinosum, granulosum, and corneum. As an alternative, human skin equivalents such as reconstructed human epidermis (RHE) can serve as functional test systems to study wound healing on a cellular level. RHE reveals all of these layers and has already been used as a test system in multiple applications such as risk assessment (Kandárová et al., 2006; Schäfer-Korting et al., 2008). Moreover, reepithelialization has been investigated in these models but also in wound healing studies *in vitro* (Chen et al., 2014; Deshayes et al., 2018; Egles et al., 2010; Safferling et al., 2013). A popular technique to generate wounds in 3D RHE is, similar to 2D cell

* Corresponding author. Translational Center for Regenerative Therapies TLZ-RT, Fraunhofer-Institute for Silicate Research ISC, Neunerplatz 2, 97082, Würzburg, Germany.
E-mail address: lisa.kiesewetter@isc.fraunhofer.de (L. Kiesewetter).

https://doi.org/10.1016/j.bios.2019.111555
Received 24 June 2019; Received in revised form 26 July 2019; Accepted 29 July 2019
Available online 01 August 2019
0956-5663/

culture models, by the positioning of a place holder or spacer in the middle of the skin equivalent, leaving a circle-shaped hole cell-free during tissue maturation (Bullock et al., 2007; Deshayes et al., 2018). Despite the advantage that the thin and easily breaking cell culture membrane underneath the cells remains unaffected, no actual wounding takes place. Hence, we suspect activation of keratinocytes to be different since an actual process of wounding is missing.

Here, we introduce a new *in vitro* model for epidermal wound healing (EWH) based on RHE grown on a cell culture membrane. Following tissue maturation, the RHE models are wounded using a biopsy punch. Apart from standard analysis techniques such as monitoring of ongoing wound closure in phase contrast and laser scanning microscopy as well as in histological staining of cross sections, we present impedance spectroscopy (Groeber et al., 2015) as a sensitive tool to quantitatively measure the wound closure and the restoration of the epidermal barrier. With this method, it is now possible to observe the development of the skin barrier non-destructively for each model over a culture time of 14 days post wounding.

2. Materials and methods

2.1. Generation of wounded reconstructed human epidermis

For the generation of RHE, human epidermal keratinocytes (hEK) were isolated from foreskin biopsies obtained from juvenile donors under informed consent according to ethical approval granted by the local ethical committee (approval number IGBZSF-2012-078) and the written confirmed consent of their guardians. Following the isolation of keratinocytes according to a previously described process (Groeber et al., 2016), cells were cultured in EpiLife® medium supplemented with Human Keratinocyte Growth Supplements and 1% penicillin/streptomycin (all from Life Technologies, Germany) in a humidified incubator at 37 °C and 5% CO_2 up to passage two. RHE models were generated according to the open source method described by Groeber et al., (2016). In brief, hEK were detached, suspended in EpiLife® medium supplemented with Human Keratinocyte Growth Supplement, 1% penicillin/streptomycin and 1.44 mM calcium chloride (Sigma-Aldrich, Germany), and seeded on 12-well transwell inserts (0.4 µm pore size; Greiner Bio-One GmbH, Germany) at a total cell count of 5×10^5 hEK per insert. After 24 h culture at submerged conditions, the RHE cultures were shifted to air-lift culture and the cell culture medium was exchanged to EpiLife® air-liquid-interface medium additionally supplemented with 73 µg/ml L-ascorbic acid 2-phosphate and 10 ng/ml keratinocyte growth factor (both from Sigma-Aldrich, Germany). RHE models were cultured for 14 days and medium was changed three times a week. On day 14, RHEs were injured locally in the center of the insert without destroying the cell culture membrane using dermal biopsy punches with diameters between 2 and 8 mm (pfm medical ag, Germany). For detaching the wounded area, the models were incubated on 0.05% Trypsin/EDTA (Life Technologies, Germany) for 2.5 min and washed thoroughly with fetal calf serum (Biochrom, Germany) and EpiLife® medium. The resulting wounded reconstructed human epidermis (wRHE) models were kept in culture for another 14 days with medium renewed three times a week.

2.2. Impedance spectroscopy and analysis

For impedance spectroscopy measurement, RHEs and wRHEs were positioned between a working (1.04 cm^2 surface area) and a counter (4.52 cm^2) electrode in a custom-made measuring system with stainless steel or nanostructured titanium nitride (TiN) electrodes previously described (Groeber et al., 2015; Schmitz et al., 2018). To achieve electrical coupling between the tissue and the electrodes, the inner and outer compartments were filled with EpiLife® medium supplemented with 1% penicillin/streptomycin and 1.44 mM calcium chloride. Impedance was measured with the impedance spectrometer LCR HiTESTER 3522–50 (HIOKI E.E. Corporation, Japan) in a frequency range from 1 Hz to 100 kHz with 40 sampling points logarithmically distributed over the spectrum by applying a sinusoidal alternating current perturbation signal with 0.2 V limited to 3 mA. The measurement was operated with a custom-made LabVIEW user interface (National Instruments, USA). Impedance measurements were performed on day 14 of RHE culture before wounding as well as directly after wounding, and repeated on day 1, 3, 7, 10, and 14 after wounding. Impedance data was analyzed following three different approaches. First, the $TEER_{1000\ Hz}$ (in Ωcm^2) was calculated by linear regression of the impedance spectrum after clearing out the blank spectrum for an empty cell culture membrane without RHE and subsequent multiplication of the impedance Z (in Ω) at 1000 Hz by the culture area of the RHE (1.13 cm^2). Second, an equivalent circuit modeling the biological system was fitted employing a complex non-linear least squares algorithm in MATLAB (MathWorks, USA). In doing so, the tissue's resistance R_{RHE} (in Ω) and capacitance C_{RHE} (in µF) were obtained (Groeber et al., 2015). Third, a single characteristic frequency $f_{c,s}$ (in Hz) was calculated according to White et al., only in our case at the maximum difference of the measured amplitude ΔA of the impedance or the maximum difference of the measured absolute impedance ΔZ and the corresponding spectrum of the blank measurement (White et al., 2013). The computed $f_{c,s}$ was compared for RHE and wRHE with different wound sizes as well as for both electrode materials applied in this study.

2.3. Imaging of wound area and reepithelialization

The quality of the generated wounds and the subsequent re-epithelialization of the wound area was monitored employing phase-contrast microscopy. Cultures of wRHE were put in a sterile petri dish and photos of the wound area were taken directly after wounding and on the following days until wound closure, using a 4-fold objective with matching phase filter at the EVOS® XL Core (Life Technologies, Germany). Wound area, the mean Feret diameter, roundness and circularity of the wound were determined with NIH ImageJ software (National Institute of Health, USA), whereby wound perimeters were encircled with the freehand selection tool. Surface topography scanning of the wRHE in micrometer range was performed with VK-X210 3D Laser Microscope (Keyence Corporation, Japan) enabling three-dimensional optical and geometrical analysis. Pictures were taken with a violet laser of 408 nm wavelength and an objective lens with 20x magnification. Image analysis was performed using the VKX100/200 Analyzer Software (Keyence Corporation, Japan). Geometrical analysis enabled measurement of 3D parameters such the wound volume that cannot be assessed using 2D phase-contrast microscopy.

2.4. Measurement of glucose and lactate concentration as well as lactate dehydrogenase liberation in cell culture medium

Additionally, glucose and lactate concentrations of RHE and wRHE media were measured to reveal possible influences of wounding and wound closure on glucose consumption and lactate production. Besides, lactate dehydrogenase (LDH) liberation was determined as a marker for cell degradation. For collecting supernatants of wRHE and RHE, models were exposed to 1 ml fresh cell culture medium for 24 h. Medium samples were taken directly before wounding (d0), as well as on day 1 (24 h after wounding), 3, 7, 10, and 14 after injury. LDH liberation, glucose and lactate concentrations were measured using the Cedex Bio Analyzer (Roche Diagnostics GmbH, Germany). By subtracting the measured glucose concentrations from the medium baseline concentration (6.44 mM), the glucose consumption (in mM for 24 h) was calculated. To elucidate the rate of glucose consumption compared to lactate production, the lactate concentration (in mM for 24 h) was subtracted from the obtained glucose consumption.

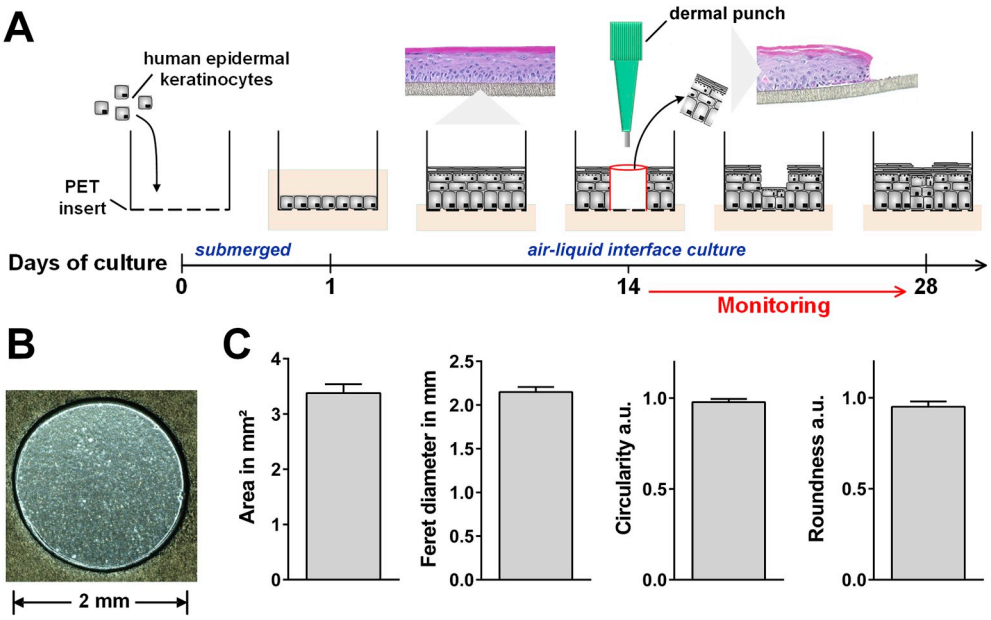

Fig. 1. Generation and culture of standardized wounded reconstructed human epidermis.
A: Scheme for generating and culture of wounded reconstructed human epidermis (wRHE). Models were wounded on day 14 of culture using a dermal punch and kept in culture for monitoring of wound closure for another 14 days. B: Phase-contrast microscopy image of wound generated with 2 mm dermal punch. After removal of the tissue within the wound area only the blank membrane was left and the wound margin is visible, allowing analysis of wound geometry. C: Results of geometrical analysis of 50 wounds (2 mm diameter). All parameters, wound area, Feret diameter, circularity and roundness, showed robust values with only small standard deviations (n = 50; mean values ± SD).

2.5. Histological staining and immunofluorescence

At multiple time points during culture, wRHE models were fixed in Roti Histofix® (Carl Roth GmbH, Germany) and embedded in paraffin before cutting 3 µm cross sections for histological staining. Hematoxylin & eosin (H&E; Morphisto, Germany) staining allowed for assessment of the general morphological architecture on bright-field images, obtained by a KEYENCE BZ 9000 microscope (Keyence Corporation, Japan). Three consecutive images were taken to generate a merged overview image of the whole wound region, showing approximately 25% surrounding tissue at the wound margin, and 75% wound area. For immunofluorescence staining tissue sections were hydrated. In case of primary antibodies E-cadherin and claudin-1, the sections were subjected to antigen retrieval in citrate buffer at pH 6 and 100 °C for 25 min. Unspecific binding sites were blocked with 5% donkey serum (Life Technologies, Germany) for 20 min. The primary antibody solutions (keratin 10 (K10), 1:100 (Abcam, United Kingdom); keratin 14 (K14), 1:1000 (Sigma-Aldrich, Germany); keratin 17 (K17), 1:500 (Abcam, United Kingdom); E-cadherin, 1:100 (BD Biosciences, United States of America); claudin-1, 1:600 (Life Technologies, Germany)) were applied and incubated for 16 h at 4 °C, followed by the incubation of the secondary antibody solutions coupled with Alexa Fluor® 647 or Alexa Fluor® 488 (donkey anti rabbit or donkey anti mouse; all from Life Technologies, Germany) for 60 min at room temperature. After washing, the cell nuclei were counterstained with 4',6-diamidino-2-phenylindole (DAPI) in Fluoromount-G DAPI mounting medium (Life Technologies, Germany) and fluorescence images were taken employing the KEYENCE BZ 9000 microscope.

2.6. Statistical analysis

All impedance data was tested for normality using the Shapiro-Wilk test. If normality was proven, one-way or two-way ANOVA employing Dunnett's, Tukey's or Sidak's multiple comparisons test was performed for analysis of quantitative data, whereby a p-value < 0.05 was considered significant. Depending on the experiment, statistics were either calculated comparing the states directly before or after wounding, or between the different data sets. The data shows mean values for 4 to 50 technical replicates of three independent test runs (3 donors), if not stated differently. Repeatability between technical replicates and independent test runs is depicted as standard deviation. The specific statistical test for each analysis is stated in the respective figure captions. Statistics were computed in GraphPad PRISM 6 software (GraphPad Software Inc., USA).

3. Results

3.1. Standardized wounds can be generated in reconstructed human epidermis using a biopsy punch

After fourteen days of tissue maturation at the air-liquid interface, RHEs were injured locally using dermal punches of varying diameters and kept in culture for another two weeks (Fig. 1 A). To quantify the repeatability of the process, images of the resulting wounds were taken with phase-contrast microscopy and subjected to image analysis (Fig. 1 B).

Fig. 1 C depicts the results for 50 wounds generated with the 2 mm dermal punch (theoretical wound area 3.14 mm^2), showing consistent values for all wounds with a mean wound area of 3.41 mm^2 and 2.15 mm Feret diameter, a measure for the distance between two parallel lines tangential to the wound area. Additionally, mean circularity and roundness of 0.98 and 0.95 were calculated according to equations (1) and (2). Between all generated wounds only little derivations can be observed resulting in standard deviations of 0.162 for the area, 0.059 for the Feret diameter, 0.018 for circularity, and 0.029 for roundness.

$$circularity = \frac{\pi \cdot 4 \cdot wound\ area}{wound\ perimeter^2} \quad (1)$$

$$roundness = \frac{4 \cdot wound\ area}{\pi \cdot Feret\ diameter^2} \quad (2)$$

3.2. Increasing wound diameters can be detected via impedance spectroscopy

To test, whether impedance spectroscopy is sensitive enough to detect tissue defects of different sizes in RHE, wounds were generated with increasing diameters. Starting with 2 mm (2.8% of total culture area), then 3 mm (6.3%), followed by 4 mm (11.1%), 5 mm (17.4%), 6 mm (25.0%), and finally 8 mm, the wound size was increased up to 44.4% of the culture area. Impedance was measured directly before wounding and after each wounding step. After subtraction of the measured values for an empty cell culture membrane, the $TEER_{1000\ Hz}$ in kΩcm² was calculated that showed to be a predictive value to three

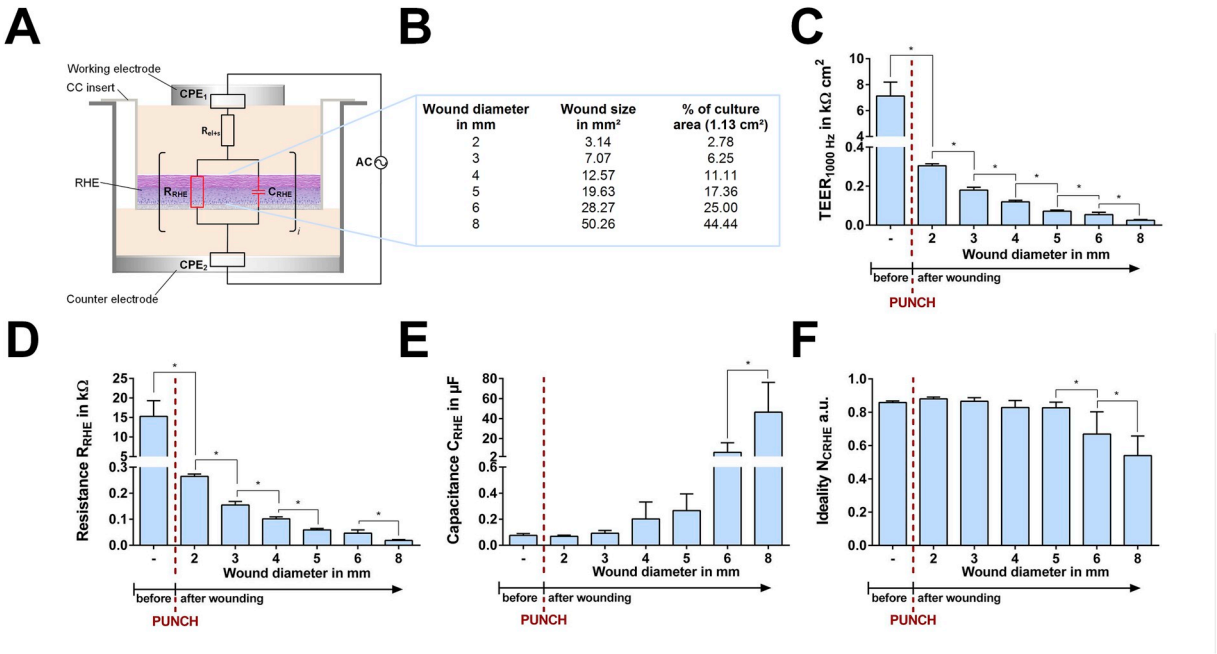

Fig. 2. Impedance spectroscopy allows detection of different wound sizes.A: The equivalent circuit used to fit the measured impedance spectra of the reconstructed human epidermis (RHE) models. B: List of different wound diameters and the consequent wound sizes. C–F show the results for transepithelial electrical resistances $TEER_{1000\ Hz}$ (C), fitted resistances R_{RHE} (D) and capacitances C_{RHE} (E) with ideality N_{CRHE} (F) of reconstructed human epidermis wounded repeatedly with dermal punches with increasing diameters. Data shown in comparison to levels measured directly before wounding. $TEER_{1000\ Hz}$ and R_{RHE} dropped significantly following injury and decreased further with increasing wound diameter. C_{RHE} was only altered slightly by wound sizes of 2–5 mm, but increased significantly with 6–8 mm wound diameter with growing non-ideality of the capacity (n = 9; mean values ± SD; One-way ANOVA with Tukey's multiple comparisons test, $*p < 0.05$).

dimensional tissue constructs (Lotz et al., 2018). Moreover, impedance spectra were fitted using an equivalent circuit as previously described (Groeber et al., 2015) and depicted in Fig. 2 A. This analysis resulted in the R_{RHE} in kΩ, C_{RHE} in µF, and N_{CRHE} (arbitrary unit) allowing detailed analysis of the models' resistive and capacitive behavior.

With increasing wound size, the $TEER_{1000\ Hz}$ as well as the R_{RHE} decreased significantly from 7.12 kΩcm^2 to 25.24 Ωcm^2 (−99.65%) and 15.28 kΩ to 18.41 Ω (−99.88%), respectively, whereas the highest declines by −95.72% ($TEER_{1000\ Hz}$) and −98.27% (R_{RHE}) were observed after the first wounding with the 2 mm dermal punch compared to the impedance levels before wounding (Fig. 2 C and D). C_{RHE} started at 0.075 µF and only changed little (+0.19 µF) with the 2–5 mm lesions (Fig. 2 E). The enlarging of the wound diameter to 6 and 8 mm resulted in a significant jump in C_{RHE} to 6.18 and 46.35 µF, respectively. At the same time, the ideality N_{CRHE} of the capacitance decreased to 0.54, showing a growing non-ideality of the C_{RHE}. All data underlying the graphs in Fig. 2 is listed in detail in supplementary table 1.

3.3. Phase-contrast and laser scanning microscopy reveal ongoing reepithelialization over culture time

Wound closure was monitored using 2D phase-contrast microscopy. Images were taken and showed decreasing mean wound areas over 14 days (Fig. 3 A, D). Although most wounds were fully reepithelialized within 7 days, we could observe clear variances between the donors (supplementary figure 6 A). Taking the mean wound area on day 0 of 3.41 mm^2 and the average area of 1.79 mm^2 on day 3, the re-epithelialization rate can be calculated according to Laplante et al., resulting in 171 µm per day (Laplante et al., 2001).

To get insights on the volume of the lesions, the surface of seven wounds was scanned over 14 days of culture post wounding via laser scanning microscopy (Fig. 3 B, C, E). The 3D images confirmed mostly completed wound healing in one week, whereby the maximum depth of the wound, noted at the front edge of the 3D images in Fig. 3 C, continued to decrease remarkably from day 0 to day 7, reaching the unwounded level (yellow color code) on day 7 after wounding. This development was concomitant with the decreasing wound area and wound volume calculated from the 3D images (Fig. 3 E). Nevertheless, the wound margin was still visible (red circle), as an elevated area after full wound closure on day 14 (Fig. 3 C).

3.4. Histological analysis shows progress of reepithelialization

The images of cross sections of wRHEs through the wound centers showed the ongoing wound closure with culture time after wounding (Fig. 4). Directly after wounding the wound edge was clearly visible while only the stratum corneum showed the original cutting edge within the following days. Most wounds were fully closed between day 3 and 7 after wounding with one or more cell layers in the wound center. Starting from the wound edges, keratinocytes began to differentiate within the wound, forming the characteristic epidermal layers proven with immunofluorescence staining for basal keratinocyte marker keratin 14 (K14) in combination with the differentiation marker keratin 10 (K10). Positive staining for keratin 17 (K17), a marker for activated, migrating hEK (Freedberg et al., 2001; McGowan and Coulombe, 1998; Paladini et al., 1996) showed up at the wound edges between day 0 and 3 after wounding and disappeared during further culture. In addition to the shown images, Supplementary Figs. 3 and 4 present the absence of positive staining offside the wound and staining for cell-cell-adhesion (E-cadherin) and tight-junctions markers (claudin-1).

3.5. Wounding and ongoing reepithelization influence metabolic activity of keratinocytes

The relation between glucose consumption and lactate liberation

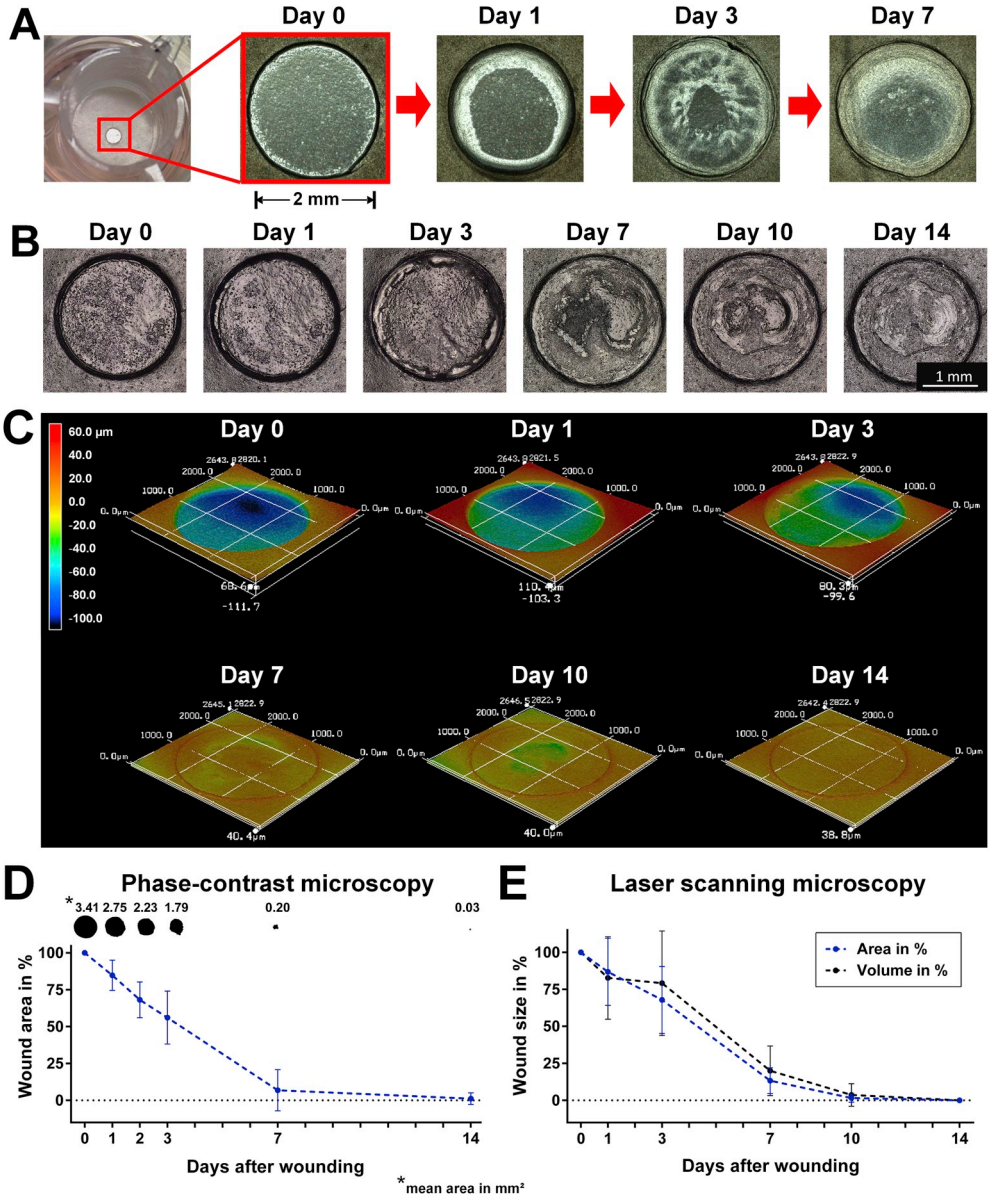

Fig. 3. Wound closure can be observed in phase-contrast and laser scanning microscopy.
A: Exemplary phase-contrast microscopy images of wound region for wounded epidermal model over culture time post wounding. B: Representative laser scans of the lesion site in wRHE over culture time after wounding. C: 3D display of the wound region of wRHE from the day of wounding until day 14 post wounding. The color code signifies the depth of the wounds according to the color scale on the left defined according to a reference point on the intact tissue. D: Mean wound area in percentage of initial wound size for 21 wounds (3 biological and 7 technical replicates) taken from phase-contrast microscopy images. The black spots above the chart show mean wound sizes in mm^2. E: 3D laser scanning microscopy led to mean wound area and wound volume in percentage of initial lesion size for seven wounds. Wound closure was almost completed between day 7 and 14 after wounding, major progress happening in the first seven days after injury. Mean values ± SD. . (For interpretation of the references to color in this figure legend, the reader is referred to the Web version of this article.)

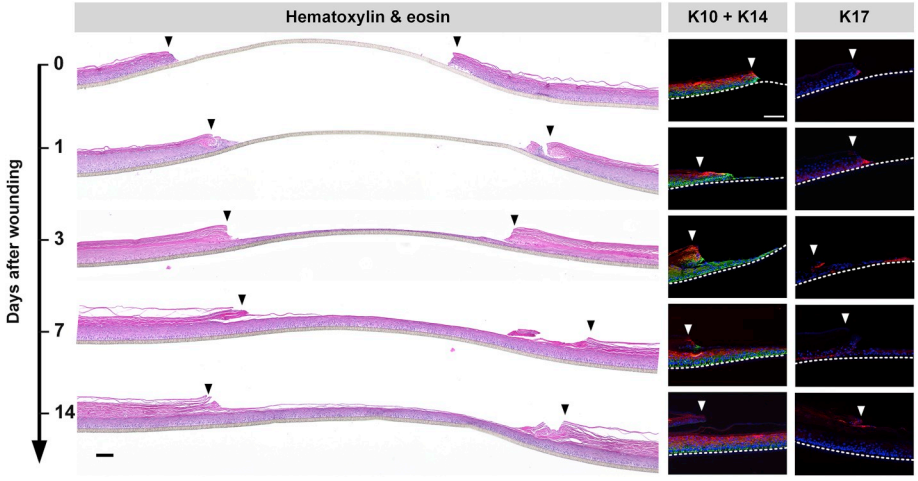

Fig. 4. Histological analysis of wound closure over time.
Hematoxylin and eosin staining of cross sections showing the center of wounds with 2 mm diameter with ingrowing keratinocytes already one day after wounding. Between day 3 and 7, most wounds were closed with one or multiple layers of cells. Immunofluorescence staining of the wound edges visualizes the differentiation of the keratinocytes within the wound over culture time in markers for keratin 10 (K10, red) and keratin 14 (K14, green). Positive staining for keratin 17 (K17, red) shows activated keratinocytes at the wound borders. Cell nuclei are labeled with DAPI. Arrow heads point to the cutting edges of the wounds, white dashed lines indicate the cell culture membrane. All scale bars indicate 100 µm.

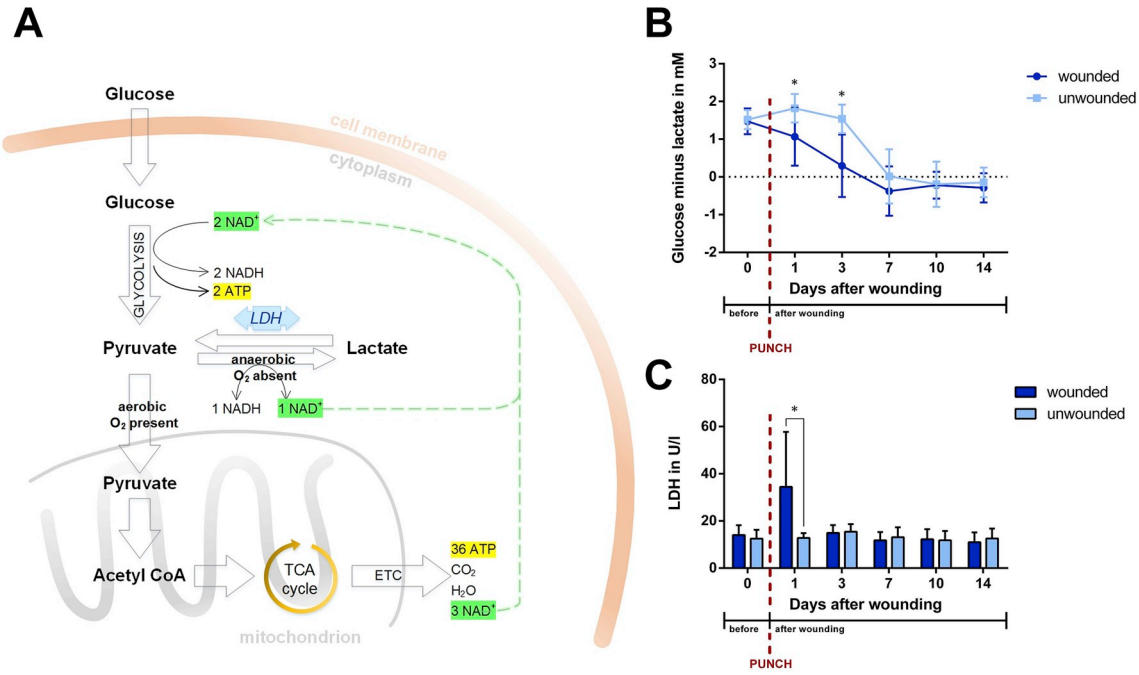

Fig. 5. Wounding causes metabolic stress in reconstructed human epidermis. A: Schematic drawing of glucose metabolism depending on the presence of oxygen according to Phypers and Pierce. In case of aerobic conditions, the intermediate metabolite pyruvate is converted to acetyl CoA and further oxidized in the tricarboxylic acid cycle (TCA) and the electron transport chain (ETC) to carbon dioxide and water, energy-rich adenosine triphosphate (ATP) and nicotinamide adenine dinucleotide (NAD^+). Under anaerobic conditions or in case of cellular stress, the metabolic balance is shifted towards lactic acid fermentation and glucose is converted reversibly via the enzyme lactate dehydrogenase (LDH) to lactate and NAD^+ (adapted from Phypers and Pierce, 2006). B: Difference of glucose consumption and lactate production of wounded and unwounded models over culture time after wounding. The glucose consumption is computed using the total glucose concentration of the cell culture medium (6.44 mM) and subtracting the glucose concentration measured at the distinct time point. Wounding results in higher values for lactate production, causing a significant shift towards lower ratios for wounded models compared to unwounded models in the first days after wounding. C: Levels of LDH for wounded and unwounded models in cell culture supernatant showing a significant peak in LDH liberation after wounding. Mean values and standard deviations shown for 3 biological and 4 technical replicates. Significances were calculated using two-way ANOVA with Sidak's multiple comparisons test, $*p < 0.05$.

can give information about metabolic activity of cells and, in case of imbalances, reveal presence of cellular stress caused by e.g. sudden need of energy-devouring proliferation or migration processes. Under anaerobic conditions or if suddenly a higher amount of energy-rich ATP is needed than can be supplied via the glycolysis, the enzyme lactate dehydrogenase catalyzes the reversible conversion of pyruvate to lactic acid (Fig. 5 A) to recycle NAD^+ via the oxidization of NADH, which is then available again for the glycolysis (Phypers and Pierce, 2006).

Within the supernatant of RHE and wRHE models, the glucose consumption and lactate production was determined (see Supplementary Fig. 5 for data for each donor underlying the graphs in Fig. 5 B and C, supplementary tables 3-5 list all data underlying Fig. 5 B and C) and used to calculate the relation between both values by subtracting the lactate production from the glucose consumption (Fig. 5 B).

Starting from the same level before wounding with a mean ratio of 1.5 mM of glucose consumption and lactate production, the wRHE models produced significantly more lactate than the unwounded RHE models shifting the ratio to lower values for the wRHE, whereby donor specific differences could be seen in changes of glucose consumption and lactate production (see Supplementary Fig. 5). Fig. 5 C depicts the average LDH levels measured in the cell culture supernatant, showing a significant increase for wRHE in the first 24 h after wounding. However, in the following days after wounding, the level of LDH stayed well beneath the test range of 20 U/l.

3.6. Reepithelialization can be monitored using impedance spectroscopy

Employing impedance spectroscopy, the epidermal barrier was estimated for three donors with 7 wRHE models each over a two-week culture time post injury. Directly after wounding with the 2 mm biopsy punch, impedance levels decreased significantly for both, $TEER_{1000\ Hz}$ and R_{RHE}, by −97.0% and −99.4%, respectively (Fig. 6A–B).

As seen for the analysis of different wound sizes (Supplementary Fig. 2), $f_{c,s}$ leaped to higher values around 1145 Hz with the 2 mm lesion (Fig. 6 D). With further culture of the wRHE models, the $TEER_{1000\ Hz}$ increased again closing at 105.8% of the initial $TEER_{1000\ Hz}$ measured directly before wounding. R_{RHE} remained lower with an average value of 52.6% of the initial mean value 14 days after wounding (Fig. 6 B). In the same time, $f_{c,s}$ decreased back to the initial level at 29 Hz, whereby the strongest decline was measured between day 3 and 7 after wounding, similar to the progress in $TEER_{1000\ Hz}$ and R_{RHE}, whereby changes from day 0 to day 1 and 3 were already significant. On the contrary, wounding did not alter the levels of C_{RHE} while comparing results from directly before and after injury (Fig. 6 C). Here, shifting towards higher levels of C_{RHE} was detected during the first 7 days after wounding with peak values on day 7 (0.32 µF ± 0.23, equaling 531.6% of mean C_{RHE} before wounding). Major changes could be observed between day 3 and 7 post injury as it was also the case for $TEER_{1000\ Hz}$ and R_{RHE}. In the second week of culture after wounding, C_{RHE} dropped again to comparable levels as measured directly before wounding (110.5% of initial capacitances). Supplementary Fig. 6 reveals small differences in the recovery of the epidermal barrier for wRHE of three different donors. All impedance data are listed in detail in supplementary tables 6-8.

4. Discussion

RHE models have been widely used as test models for risk assessment and have shown to be a highly predictive alternative to classical animal models. However, these models have not yet been established for efficacy testing of pharmaceutical compounds intended to foster wound healing. Although these models still lack an active immune

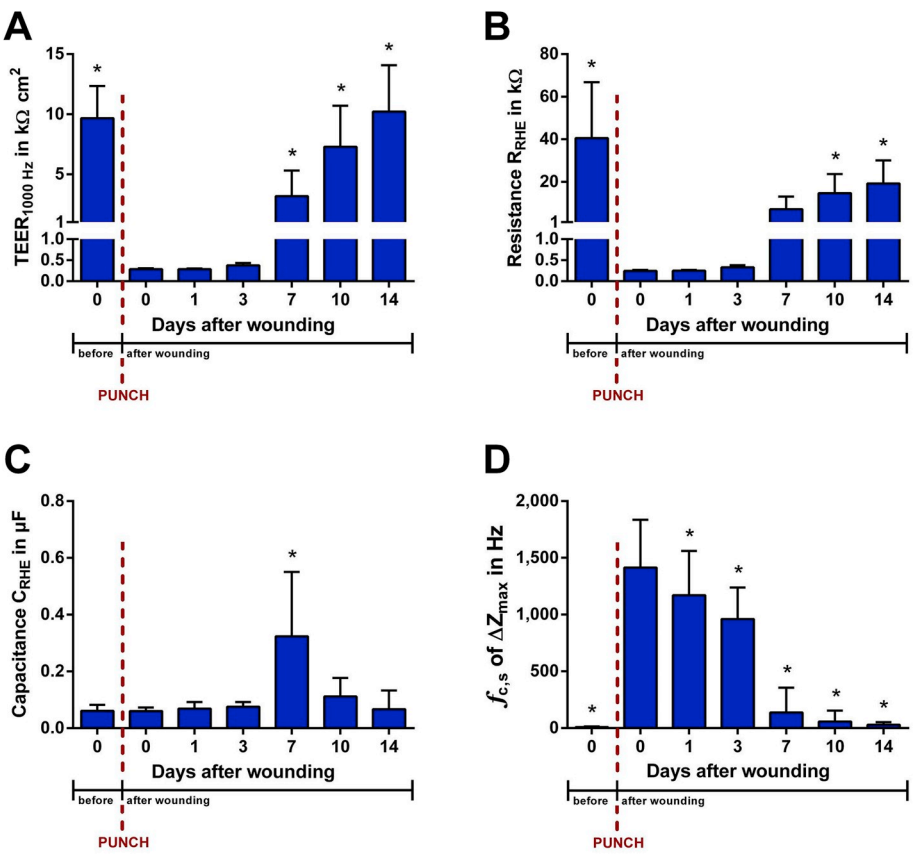

Fig. 6. Reepithelialization can be monitored non-invasively using impedance spectroscopy.
Mean results for transepithelial electrical resistance $TEER_{1000\ Hz}$ (A), fitted resistance R_{RHE} (B) and capacitance C_{RHE} (C) for 7 wounded epidermal models of three donors. The models were wounded on day 14 of culture and impedance spectroscopy was performed on multiple days during a two-week culture post injury. All significances show comparisons to day 0 after wounding. Both, $TEER_{1000\ Hz}$ and R_{RHE} show significant decreases caused by the local lesion as well as significant increases of impedance levels over culture time with endpoint levels on day 28 of culture (day 14 post wounding) similar to the state before wounding. C_{RHE} resulted in significant increases within the first week of culture after wounding and decreasing levels during the second week after wounding. Analysis of the single characteristic frequency $f_{c,s}$ (D) revealed decreasing frequencies over time during reepithelialization, ending at a level similar to $f_{c,s}$ before wounding, whereby most changes happened between day 3 and 7 comparable to $TEER_{1000\ Hz}$ and R_{RHE}. (3 biological and 7 technical replicates, mean value ± SD; one-way ANOVA with Dunnett's multiple comparisons test, $^*p < 0.05$).

system and a dermal compartment, they provide a unique possibility to investigate the response of keratinocytes in a highly controlled experimental setup. Thus, the aim of this study was to establish RHE with defined wounds that can be employed to investigate reepithelialization.

4.1. Mechanical wounding using biopsy punches generates standardized wounds in RHE models and elicits metabolic changes within keratinocytes

Following maturation, RHEs were wounded locally using a 2 mm biopsy punch, which we could first demonstrate to be feasible using RHE. With a surface area of 3.4 mm^2, the wound area is approximately 3% of the total surface of the model. The generated wounds were highly repeatable and represent a low-cost alternative to other accurate techniques requiring expensive laboratory infrastructure, such as laser ablation (Marquardt et al., 2015; Stamm et al., 2016). Histological staining revealed a good quality of the epidermal architecture and an intact cell culture membrane. Interestingly, the wound had a direct effect on the keratinocytes resulting in a beginning healing process already after 24 h with first cells growing into the wound area in the histological cross section staining. Cellular activation of cells at the wound edge is shown by the presence of keratin 17 known to promote contractility and facilitating migration (Freedberg et al., 2001; McGowan and Coulombe, 1998; Paladini et al., 1996). Along with the first days after wounding, the glucose to lactate ratio in the cell culture medium decreased significantly, indicating an adaption of the keratinocytes' cell metabolism towards a stress-induced "anaerobic" metabolism. With progressing wound closure, the cellular metabolism returned to values similar to the control group of unwounded RHE around day 7 after wounding. This could be a sign for less stress-associated metabolism, since the wounds were mostly completely closed and an ad-hoc high proliferative and migration action is not needed anymore. A signal promoting the swift response by the keratinocytes might be soluble factors such as LDH, for which we could see an increased concentration directly after wounding. Moreover, a change of the transepithelial potential as reported by Dubé et al. might be an additional biophysical cue responsible for the onset of the reepithelialization (Dube et al., 2010). Since, the wounding of the models seems to elicit a specific cellular response, we think that a wounding of the models is critical and that a generation of models with pre-formed holes is significantly different to an acute wound situation.

4.2. Characterization of wounds using imaging tools and impedance spectroscopy

The decreasing wound area during reepithelialization was measured using 2D phase-contrast microscopy and 3D laser scanning imaging. Using topographical laser scanning microscopy we could determine that the entire wound area was covered by a monolayer of cells after seven days and the wound volume decreased to 20% (± 16.8%). Although laser scanning microscopy enabled us to monitor wound closure, no quantitative data regarding tissue structure or barrier integrity could be derived, being important parameters for describing tissue functionality. Hence, we chose impedance spectroscopy as an additional non-invasive and straightforward measuring technique for quantitative assessment of the epidermal barrier (Groeber et al., 2015; Lotz et al., 2018). Impedance spectroscopy performed directly before injury first of all ensured good quality of our RHE models with $TEER_{1000\ Hz}$ between 5 and 12 kΩcm^2. As previously demonstrated, RHE on day 14 of culture shows fully differentiated epidermal layers with high impedance levels. In the equivalent circuit for fitting of impedance data, these matured RHE models can be described using one parallel connection of a resistance and a non-ideal capacitance, whereby the ideality of the capacitor can be a measure of the surface roughness. Low capacitance levels can be referred to the high capacitor thickness of matured RHEs (Groeber et al., 2015). Since this technique works non-destructively, the same RHE models can be measured several times in row, e.g. before and

after wounding.

To assess if impedance spectroscopy is sensitive enough to detect local defects in RHEs, we measured impedance levels directly before and repeatedly after wounding with increasing wound diameters from 2 to 8 mm. $TEER_{1000\ Hz}$ and R_{RHE} showed significantly decreasing impedance levels with every enlargement in wound size demonstrating the high sensitivity to detect even small variances in wound size. The capacitance did not change significantly for the 2–5 mm wound defects. By increasing the wound diameter from 5 to 6 and 8 mm, the capacitance increased significantly. With the loss of major parts of the model for the 8 mm wound defects the total capacitor thickness of the RHE, behaving reciprocally to the magnitude of the capacitance, decreases (Groeber et al., 2015). The electrode surfaces are large compared to the wound size and the total culture area. As major parts of the tissue had been removed, most of the alternating current signal were short-circuited via the open wound, which is essentially the cell-free membrane. The highly porous insert membrane in the wound is characterized by a high surface roughness, a negligibly low capacitance and only a small resistance. Since the equivalent circuit applied in our study does not differ between the wound and the intact tissue, the results of the capacitance and the ideality represent mean values over the whole insert area, including the rim of the intact model and the wound. In order to distinguish between the wound and the intact model surrounding it, the equivalent circuit could be expanded by a resistance R_{wound} in parallel to R_{RHE} such as proposed by White et al., (2013).

Besides measuring $TEER_{1000\ Hz}$ and R_{RHE}, White et al. introduced a single characteristic frequency $f_{c,s}$, indicated, in our case of application, by the maximum difference between the measured impedance and a blank reference spectrum. According to White et al., $f_{c,s}$ increases with the increasing number of pinholes in their model. Similar to these observations we could see that $f_{c,s}$ also increases with the growing diameter of the wound for both electrode materials. This frequency-dependent behavior of the impedance for wounded skin shows the importance of not only regarding one *TEER* value at a frequency of choice, but analyzing the full impedance and phase angle spectrum, e.g. by fitting an equivalent circuit. Overall, our results show that impedance spectroscopy is sensitive enough to detect wound defects in matured RHE cultures.

4.3. Reepithelialization can be monitored non-invasively employing impedance spectroscopy

Over a time period of fourteen days after wounding, the impedance of wRHE of three donors was measured repeatedly and the $TEER_{1000\ Hz}$, R_{RHE}, and C_{RHE} results were compared to the values before and directly after wounding. Models of all donors increased in impedance values with most changes happening between day 3 and day 7 after wounding concurrent to the major progress in wound closure seen in the H&E staining of cross sections. Two weeks after wounding, impedance levels were recovered to comparable levels as before wounding. As seen in H&E staining of cross sections of wRHE models, the wound areas were fully closed and all the epidermal layers except for the stratum corneum were of comparable thickness to the intact epidermis surrounding the wounds. With the development of the lipid-rich stratum corneum in the wound area, the wRHE models regained in barrier function leading to the increase in the impedance levels. The single characteristic frequency $f_{c,s}$ went back to low frequencies similar to before wounding, again with most changes happening between day 3 and 7 after wounding, but changes already detectable within the first days after wounding. In contrast to the $TEER_{1000\ Hz}$ and the R_{RHE} values, the capacitance C_{RHE} did not change after wounding and remained constant until day 3, where, according to phase-contrast microscopy and H&E images, the wound was still partially open. Seven days after wounding, the high peak and following decreasing behavior of C_{RHE} until day 14 can be explained by the increasing capacitor thickness. Starting with a thin monolayer in the center of the lesion on day 7 after wounding, the growing cell layers in the wound during reepithelialization and the reciprocal relation between capacitance and capacitor thickness (Groeber et al., 2015) effect this decreasing capacitance to a final value similar to the initial capacitance before wounding. The high standard deviation of the capacitance on day 7 after wounding shows the non-uniform progress of wound closure for the different models. The wound is still dominating the progress of the electric field, as the thinner newly formed epidermis within the wound area is characterized by a smaller impedance than the surrounding intact tissue. Thus, the higher capacitance of the thinner tissue is overweighing the otherwise low capacitance of the intact tissue surrounding the wound. Although all donors showed proper reepithelialization in all aspects of this study, wound healing efficacy proved to be donor-dependent in terms of reepithelialization rate, imbalance of glucose consumption and lactate production, as well as recovery of the skin barrier.

Non-invasive monitoring of wound closure by electrotechnical methods for *in vitro* skin models has been described before for other electrical parameters. For example, Dubé et al. showed that the transepithelial potential can be used as a quantitative tool to measure wound closure based on the characteristic endogenous electric field of skin (Dube et al., 2010). However, their approach required larger model sizes and wound diameters (6 mm), as the electrode had to be positioned in the center of the wound. Here, impedance spectroscopy has decisive advantages. It can be applied for rapid screening of high numbers of technical replicates without the need for multiple measurement points per model. In addition, the total size of the model as well as the wound diameter are reduced to a minimum, lowering experimental costs. The concept of observing wound healing via impedance is not completely new. In the past, *in vivo* studies using bioimpedance measurement with adhesive electrodes on e.g. needle puncture or scratch wounds showed the applicability of impedance to determine the state of wound healing (Kekonen et al. 2015, 2017; Solmaz et al., 2016). So far, 2D *in vitro* studies working with impedance spectroscopy to analyze wound healing were limited to HaCaT cells grown directly on electrode surfaces and thus lacking the 3D architecture of human epidermis (Cui et al., 2017; Mondal et al., 2016). To our knowledge, this is the first *in vitro* study on epidermal wound healing employing 3D reconstructed human epidermis and impedance spectroscopy as a tool to monitor reepithelialization non-invasively by focusing on the epidermal barrier as a key function of intact skin.

5. Conclusion

We could establish a novel *in vitro* wound model for the screening of different active compounds intended to foster the reepithelialization process. Moreover, we could demonstrate that impedance spectroscopy provides a suitable method to monitor the healing process providing information regarding wound closure, thickness of the formed epithelium and the barrier function of the healing models.

Competing interests

The authors have declared that no competing interests exist.

Funding

The study was funded by the Bavarian state and the “Fraunhofer-Gesellschaft”.

CRediT authorship contribution statement

Lisa Kiesewetter: Data curation, Investigation, Formal analysis, Methodology, Writing - original draft. **Laura Littau:** Investigation, Data curation, Writing - review & editing. **Heike Walles:** Conceptualization, Funding acquisition, Project administration, Writing - review & editing. **Aldo R. Boccaccini:** Writing - review & editing. **Florian Groeber-**

Becker: Conceptualization, Formal analysis, Funding acquisition, Methodology, Project administration, Writing - review & editing.

Declaration of competing interest

The authors declare that they have no known competing financial interests or personal relationships that could have appeared to influence the work reported in this paper.

Acknowledgements

The authors thank PD Dr. med. Andreas Kerstan and Dr. Martin Funk for proof-reading of the manuscript. Moreover, the authors thank the “Fraunhofer-Gesellschaft” and the “Bayern Fit Programm” (Grant number 100722) of the Bavarian Ministry of Economic Affairs, Energy and Technology for financially supporting this study. This publication was funded by the German Research Foundation (DFG).

Appendix A. Supplementary data

Supplementary data to this article can be found online at https://doi.org/10.1016/j.bios.2019.111555.

References

Bullock, A.J., Barker, A.T., Coulton, L., MacNeil, S., 2007. Bioelectromagnetics 28 (1), 31–41.
Chen, Z., Yang, J., Wu, B., Tawil, B., 2014. Dev. Biol. 2 (4), 198.
Chmielowiec, J., Borowiak, M., Morkel, M., Stradal, T., Munz, B., Werner, S., Wehland, J., Birchmeier, C., Birchmeier, W., 2007. J. Cell Biol. 177 (1), 151–162.
Cui, Y., An, Y., Jin, T., Zhang, F., He, P., 2017. Sens. Actuators B Chem. 250, 461–468.
Deshayes, N., Bloas, F., Boissout, F., Lecardonnel, J., Paris, M., 2018. Exp. Dermatol. 27 (5), 460–462.
Dube, J., Rochette-Drouin, O., Levesque, P., Gauvin, R., Roberge, C.J., Auger, F.A., Goulet, D., Bourdages, M., Plante, M., Germain, L., Moulin, V.J., 2010. Tissue Eng. A 16 (10), 3055–3063.
Egles, C., Garlick, J.A., Shamis, Y., 2010. Methods Mol. Biol. 585, 345–359.
Freedberg, I.M., Tomic-Canic, M., Komine, M., Blumenberg, M., 2001. J. Investig. Dermatol. 116 (5), 633–640.
Gonzalez-Andrades, M., Alonso-Pastor, L., Mauris, J., Cruzat, A., Dohlman, C.H., Argueso, P., 2016. Sci. Rep. 6, 19395.
Groeber, F., Engelhardt, L., Egger, S., Werthmann, H., Monaghan, M., Walles, H., Hansmann, J., 2015. J. Pharm. Res. 32 (5), 1845–1854.
Groeber, F., Schober, L., Schmid, F.F., Traube, A., Kolbus-Hernandez, S., Daton, K., Hoffmann, S., Petersohn, D., Schäfer-Korting, M., Walles, H., Mewes, K.R., 2016. Toxicol. In Vitro 36, 254–261.
Kandárová, H., Liebsch, M., Schmidt, E., Genschow, E., Traue, D., Spielmann, H., Meyer, K., Steinhoff, C., Tornier, C., De Wever, B., Rosdy, M., 2006. Altern Lab Anim 34 (4), 393–406.
Kekonen, A., Bergelin, M., Eriksson, J.-E., Vaalasti, A., Ylänen, H., Viik, J., 2017. Physiol. Meas. 38 (7), 1373–1383.
Kekonen, A., Bergelin, M., Eriksson, J.-E., Ylänen, H., Viik, J., 2015. Int. J. Bioelectromagn. 17 (1), 36–41.
Laplante, A.F., Germain, L., Auger, F.A., Moulin, V.J., 2001. FASEB J. 15 (13), 2377–2389.
Liang, C.-C., Park, A.Y., Guan, J.-L., 2007. Nat. Protoc. 2 (2), 329–333.
Liu, Y., Petreaca, M., Yao, M., Martins-Green, M., 2009. BMC Cell Biol. 10 (1), 1.
Lotz, C., Kiesewetter, L., Schmid, F.F., Hansmann, J., Walles, H., Groeber-Becker, F., 2018. Sci. Rep. 8 (1), 15049.
Marquardt, Y., Amann, P.M., Heise, R., Czaja, K., Steiner, T., Merk, H.F., Skazik-Voogt, C., Baron, J.M., 2015. Lasers Surg. Med. 47 (3), 257–265.
Martin, P., 1997. Science 276 (5309), 75–81.
McGowan, K.M., Coulombe, P.A., 1998. J. Cell Biol. 143 (2), 469–486.
Menger, B., Vogt, P.M., Allmeling, C., Radtke, C., Kuhbier, J.W., Reimers, K., 2011. Ann. Surg. 253 (2), 410–418.
Mondal, D., Bose, R., Chaudhuri, C.R., 2016. IEEE T NANOTECHNOL 15 (5), 791–800.
Paladini, R.D., Takahashi, K., Bravo, N.S., Coulombe, P.A., 1996. J. Cell Biol. 132 (3), 381–397.
Phypers, B., Pierce, J.M.T., 2006. Anaesth. Crit. Care Pain Med. 6 (3), 128–132.
Safferling, K., Sütterlin, T., Westphal, K., Ernst, C., Breuhahn, K., James, M., Jäger, D., Halama, N., Grabe, N., 2013. J. Cell Biol. 203 (4), 691–709.
Schäfer-Korting, M., Bock, U., Diembeck, W., Düsing, H.-J., Gamer, A., Haltner-Ukomadu, E., Hoffmann, C., Kaca, M., Kamp, H., Kersen, S., Kietzmann, M., Korting, H.C., Krächter, H.-U., Lehr, C.-M., Liebsch, M., Mehling, A., Müller-Goymann, C., Netzlaff, F., Niedorf, F., Rübbelke, M.K., Schäfer, U., Schmidt, E., Schreiber, S., Spielmann, H., Vuia, A., Weimer, M., 2008. Altern Lab Anim 36 (2), 161–187.
Schmitz, T., Schweinlin, M., Kollhoff, R.T., Engelhardt, L., Lotz, C., Groeber-Becker, F., Walles, H., Metzger, M., Hansmann, J., 2018. ACS Appl. Nano Mater. 1 (5), 2284–2293.
Solmaz, H., Dervisoglu, S., Gulsoy, M., Ulgen, Y., 2016. Lasers Med. Sci. 31 (8), 1547–1554.
Stamm, A., Reimers, K., Strauß, S., Vogt, P., Scheper, T., Pepelanova, I., 2016. BioNanoMaterials 17 (1–2), 79–97.
White, E.A., Orazem, M.E., Bunge, A.L., 2013. J. Pharm. Res. 30 (8), 2036–2049.